

---

 S U P P L E M E N T A R Y      M A T E R I A L
 

---

**Solid-state NMR of a paramagnetic DIAD-Fe(II) catalyst: sensitivity, resolution enhancement, and structure-based assignment**

*Gwendal Kervern, Guido Pintacuda, Yong Zhang, Eric Oldfield, Charbel Roukoss, Emile Kuhn, Eberhardt Herdtweck, Jean-Marie Basset, Sylvian Cadars, Anne Lesage, Christophe Coperet and Lyndon Emsley*

C o n t e n t s

**Table S1** - Crystal Data and Details of the Structure Determination for: **Compound 1**

**Table S2** - Final Coordinates and Equivalent Isotropic Thermal Parameters of the non-Hydrogen atoms for: **Compound 1**

**Table S3** - Hydrogen Atom Positions and Isotropic Thermal Parameters for: **Compound 1**

**Table S4** - (An)isotropic Thermal Parameters for: **Compound 1**

**Table S5** - Bond Distances ( $\text{\AA}$ ) for: **Compound 1**

**Table S6** - Bond Angles (Degrees) for: **Compound 1**

**Table S7** - Predicted  $^{13}\text{C}$  and  $^1\text{H}$  NMR shifts (ppm) in the iron complex **1** from a dimer calculation.

**Figure S1** - (a)  $^{13}\text{C}$  MAS NMR spectra (500 MHz) of **2**; (b)  $^1\text{H}$ - $^{13}\text{C}$  dipolar HETCOR and (c)  $^1\text{H}$  DQ CRAMPS correlations of **2**.

**Figure S2** - Comparison between two  $^1\text{H}$ - $^{13}\text{C}$  TEDOR correlations of **1**, acquired under 33 kHz (black contours) and 30 kHz (red contours) MAS ( $T=303$  K;  $B_0=11.7$  T).

**Figure S3** - Comparison between a standard  $^1\text{H}$ - $^{13}\text{C}$  TEDOR correlation of **1** (black lines) and a modified version, lacking the z-filter and spin-echo elements before  $^{13}\text{C}$  acquisition (red lines). Narrow and wide rectangles denote  $90^\circ$  and  $180^\circ$  pulses, respectively;  $\_R$  represents the rotor period. (33 kHz MAS;  $T=303$  K;  $B_0=11.7$  T).

**Figure S4** - Correlation between experimental shifts for complex **2** and calculated diamagnetic shifts for complex **1**.

**Figure S5** - Liquid-state NMR spectra of **1** dissolved in  $\text{CH}_2\text{Cl}_2$ . (a)  $^1\text{H}$  NMR; (b)  $^1\text{H}$ ,  $^{13}\text{C}$ -HMQC.

**References** - Including complete Ref. 44 from the main text.

2,3-dimethyl-1,4-[(2',6')-diisopropylphenyl]-NN'-diazadiene bis-chloride iron (**1**)  
Ellipsoids at 50%

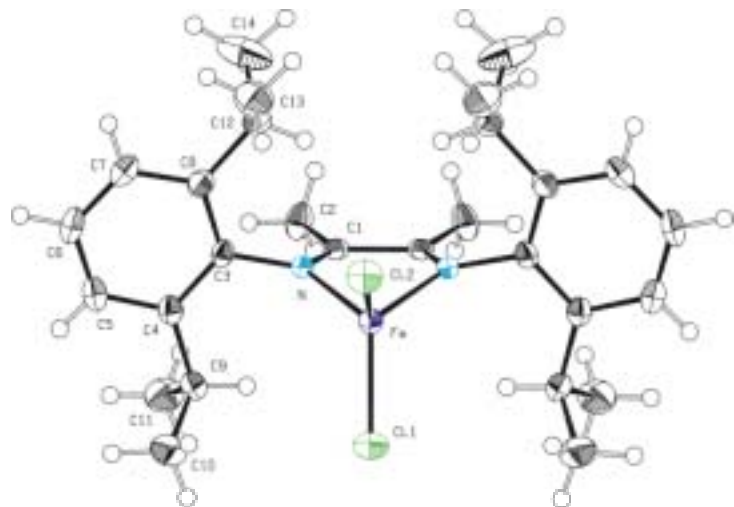


**Table S1** - Crystal Data and Details of the Structure Determination for: **Compound 1**

Crystal Data				
Formula				C28 H40 Cl2 Fe N2
Formula Weight				531.37
Crystal System				Orthorhombic
Space group		Pnma	(No. 62)	
a, b, c [Angstrom]	12.6185(2)	21.3367(3)	10.4310(1)	
V [Ang**3]			2808.41(7)	
Z				4
D(calc) [g/cm**3]				1.257
Mu(MoKa) [ /mm ]				0.745
F(000)				1128
Crystal Size [mm]		0.10 x 0.20 x	1.14	
Data Collection				
Temperature (K)				173
Radiation [Angstrom]		MoKa	0.71073	
Theta Min-Max [Deg]			1.9, 25.3	
Dataset	-15: 15 ; -25: 25 ; -12: 12			
Tot., Uniq. Data, R(int)		65010, 2646,	0.064	
Observed data [I > 2.0 sigma(I)]				2504
Refinement				
Nref, Npar				2646, 234
R, wR2, S		0.0330, 0.0716,	1.17	
Max. and Av. Shift/Error			0.00, 0.00	
Min. and Max. Resd. Dens. [e/Ang^3]			-0.24, 0.32	

**Table S2** - Final Coordinates and Equivalent Isotropic Thermal Parameters of the non-Hydrogen atoms for **Compound 1**

Atom	x	y	z	U(eq) [Ang^2]
---	---	---	---	-----
Fe	0.18492(3)	1/4	0.27977(3)	0.0201(1)
Cl1	0.14552(5)	1/4	0.07156(6)	0.0322(2)
Cl2	0.35611(5)	1/4	0.32729(7)	0.0342(2)
N	0.08962(11)	0.18902(6)	0.38814(13)	0.0177(4)
C1	0.00586(13)	0.21462(8)	0.43378(15)	0.0191(5)
C2	-0.08325(17)	0.18063(10)	0.4965(2)	0.0323(6)
C3	0.11004(13)	0.12296(8)	0.40775(17)	0.0206(5)
C4	0.07903(14)	0.07919(8)	0.31527(17)	0.0237(5)
C5	0.10540(16)	0.01646(9)	0.3379(2)	0.0311(6)
C6	0.15962(16)	-0.00136(9)	0.4465(2)	0.0329(6)
C7	0.18884(16)	0.04269(9)	0.5363(2)	0.0307(6)
C8	0.16526(14)	0.10595(9)	0.51933(18)	0.0258(5)
C9	0.01783(16)	0.09729(9)	0.19582(18)	0.0278(6)
C10	0.0769(2)	0.07882(12)	0.0741(2)	0.0436(8)
C11	-0.0932(2)	0.06883(13)	0.1979(2)	0.0437(8)
C12	0.19895(19)	0.15340(10)	0.6205(2)	0.0385(7)
C13	0.3184(2)	0.15432(14)	0.6394(3)	0.0522(9)
C14	0.1428(3)	0.1403(2)	0.7481(3)	0.0707(13)

U(eq) = 1/3 of the trace of the orthogonalized U Tensor

**Table S3** - Hydrogen Atom Positions and Isotropic Thermal Parameters for Compound 1

Atom	x	y	z	U(iso) [Ang^2]
H21	-0.0729(18)	0.1388(12)	0.492(2)	0.046(7)
H22	-0.087(2)	0.1931(13)	0.584(3)	0.070(9)
H23	-0.149(2)	0.1913(11)	0.458(2)	0.048(7)
H51	0.0837(17)	-0.0133(11)	0.281(2)	0.036(6)
H61	0.1791(17)	-0.0445(11)	0.460(2)	0.039(6)
H71	0.2267(16)	0.0302(10)	0.610(2)	0.031(5)
H91	0.0096(15)	0.1412(10)	0.1968(17)	0.022(5)
H101	0.0361(18)	0.0934(11)	-0.001(2)	0.046(7)
H102	0.147(2)	0.0978(12)	0.073(2)	0.055(8)
H103	0.084(2)	0.0315(13)	0.067(2)	0.059(8)
H111	-0.132(2)	0.0819(12)	0.124(3)	0.057(7)
H112	-0.093(2)	0.0238(14)	0.197(3)	0.066(9)
H113	-0.132(2)	0.0808(12)	0.276(3)	0.055(7)
H121	0.1781(18)	0.1925(12)	0.592(2)	0.047(7)
H131	0.337(2)	0.1868(14)	0.701(3)	0.065(8)
H132	0.340(2)	0.1158(15)	0.673(3)	0.067(9)
H133	0.356(2)	0.1629(14)	0.558(3)	0.077(10)
H141	0.161(2)	0.1751(15)	0.805(3)	0.078(10)
H142	0.072(3)	0.1404(15)	0.741(3)	0.079(10)
H143	0.178(3)	0.099(2)	0.789(4)	0.132(16)

The Temperature Factor has the Form of  $\text{Exp}(-T)$  Where  
 $T = 8 * (\text{Pi}^{**2}) * U * (\text{Sin}(\Theta) / \Lambda)^{**2}$  for Isotropic Atoms

**Table S4** - (An)isotropic Thermal Parameters for Compound 1

Atom	U(1,1) or U	U(2,2)	U(3,3)	U(2,3)	U(1,3)	U(1,2)
Fe	0.0204(2)	0.0190(2)	0.0208(2)	0	0.0043(2)	0
Cl1	0.0314(4)	0.0424(4)	0.0228(3)	0	0.0012(3)	0
Cl2	0.0221(3)	0.0420(4)	0.0385(4)	0	-0.0002(3)	0
N	0.0212(7)	0.0166(7)	0.0154(7)	-0.0001(6)	-0.0007(6)	-0.0008(6)
C1	0.0207(9)	0.0217(9)	0.0150(8)	0.0009(7)	-0.0016(7)	-0.0020(7)
C2	0.0291(11)	0.0249(10)	0.0428(12)	0.0067(9)	0.0115(10)	-0.0011(8)
C3	0.0212(8)	0.0172(8)	0.0234(9)	0.0031(7)	0.0046(7)	0.0003(7)
C4	0.0235(9)	0.0200(9)	0.0275(9)	-0.0004(7)	0.0027(7)	-0.0012(7)
C5	0.0341(11)	0.0194(9)	0.0398(11)	-0.0043(9)	0.0013(9)	-0.0017(8)
C6	0.0359(11)	0.0178(9)	0.0450(12)	0.0073(9)	0.0035(9)	0.0024(8)
C7	0.0326(10)	0.0279(10)	0.0316(11)	0.0097(8)	-0.0013(9)	0.0033(9)
C8	0.0296(10)	0.0231(9)	0.0246(9)	0.0032(8)	0.0012(8)	0.0017(7)
C9	0.0338(11)	0.0215(10)	0.0281(10)	-0.0039(8)	-0.0029(8)	-0.0012(8)
C10	0.0549(15)	0.0455(14)	0.0303(12)	-0.0054(10)	0.0016(11)	0.0047(12)
C11	0.0399(13)	0.0497(15)	0.0416(13)	0.0035(11)	-0.0126(11)	-0.0105(11)
C12	0.0588(14)	0.0283(11)	0.0284(11)	-0.0003(9)	-0.0166(10)	0.0106(10)
C13	0.0617(17)	0.0488(16)	0.0461(15)	-0.0020(13)	-0.0185(14)	-0.0118(13)
C14	0.067(2)	0.108(3)	0.0372(15)	-0.0286(17)	0.0007(14)	0.007(2)

The Temperature Factor has the Form of  $\text{Exp}(-T)$  Where  
 $T = 8 * (\text{Pi}^{**2}) * U * (\text{Sin}(\Theta) / \Lambda)^{**2}$  for Isotropic Atoms  
 $T = 2 * (\text{Pi}^{**2}) * \text{Sum}_{ij}(h(i) * h(j) * U(i,j) * A_{\text{star}}(i) * A_{\text{star}}(j))$ , for

Anisotropic Atoms.  $A_{\text{star}}(i)$  are Reciprocal Axial Lengths and  $h(i)$  are the Reflection Indices.

**Table S5** - Bond Distances (Å) for Compound 1

Fe	-C11	2.2280(7)	C2	-H21	0.90(3)
Fe	-C12	2.2163(7)	C2	-H22	0.95(3)
Fe	-N	2.1016(14)	C2	-H23	0.95(2)
N	-C1	1.281(2)	C5	-H51	0.91(2)
N	-C3	1.447(2)	C6	-H61	0.96(2)
C1	-C2	1.489(3)	C7	-H71	0.94(2)
C1	-C1_a	1.510(2)	C9	-H91	0.94(2)
C3	-C4	1.399(2)	C10	-H101	0.99(2)
C3	-C8	1.404(3)	C10	-H102	0.97(3)
C4	-C5	1.399(3)	C10	-H103	1.02(3)
C4	-C9	1.516(3)	C11	-H111	0.95(3)
C5	-C6	1.377(3)	C11	-H112	0.96(3)
C6	-C7	1.377(3)	C11	-H113	0.98(3)
C7	-C8	1.393(3)	C12	-H121	0.92(2)
C8	-C12	1.523(3)	C13	-H131	0.97(3)
C9	-C10	1.524(3)	C13	-H132	0.93(3)
C9	-C11	1.527(3)	C13	-H133	0.99(3)
C12	-C13	1.520(3)	C14	-H141	0.98(3)
C12	-C14	1.534(4)	C14	-H142	0.90(4)
			C14	-H143	1.08(4)

**Table S6** - Bond Angles (Degrees) for Compound 1

C11	-Fe	-C12	115.82(3)	C1	-C2	-H21	110.4(14)
C11	-Fe	-N	113.37(4)	C1	-C2	-H22	108.8(16)
C11	-Fe	-N_a	113.37(4)	C1	-C2	-H23	110.9(14)
C12	-Fe	-N	115.94(4)	H21	-C2	-H22	109(2)
C12	-Fe	-N_a	115.94(4)	H21	-C2	-H23	110(2)
N	-Fe	-N_a	76.50(5)	H22	-C2	-H23	107(2)
Fe	-N	-C1	114.07(11)	C4	-C5	-H51	119.0(14)
Fe	-N	-C3	125.24(11)	C6	-C5	-H51	119.5(14)
C1	-N	-C3	120.63(14)	C5	-C6	-H61	120.7(13)
N	-C1	-C2	125.33(16)	C7	-C6	-H61	119.0(13)
N	-C1	-C1_a	115.23(14)	C6	-C7	-H71	119.8(13)
C1_a	-C1	-C2	119.14(15)	C8	-C7	-H71	119.0(13)
N	-C3	-C4	120.20(15)	C4	-C9	-H91	107.5(11)
N	-C3	-C8	117.20(15)	C10	-C9	-H91	108.7(11)
C4	-C3	-C8	122.54(16)	C11	-C9	-H91	107.1(12)
C3	-C4	-C5	117.12(17)	C9	-C10	-H101	108.9(13)
C3	-C4	-C9	122.64(16)	C9	-C10	-H102	110.3(13)
C5	-C4	-C9	120.23(16)	C9	-C10	-H103	111.1(13)
C4	-C5	-C6	121.41(18)	H101	-C10	-H102	109.5(19)
C5	-C6	-C7	120.27(18)	H101	-C10	-H103	107.5(18)
C6	-C7	-C8	121.16(19)	H102	-C10	-H103	109(2)
C3	-C8	-C7	117.49(17)	C9	-C11	-H111	110.0(16)
C3	-C8	-C12	122.75(17)	C9	-C11	-H112	113.3(15)
C7	-C8	-C12	119.76(17)	C9	-C11	-H113	111.4(15)
C4	-C9	-C10	111.70(17)	H111	-C11	-H112	107(2)
C4	-C9	-C11	110.76(16)	H111	-C11	-H113	110(2)
C10	-C9	-C11	110.96(17)	H112	-C11	-H113	106(2)
C8	-C12	-C13	112.04(19)	C8	-C12	-H121	107.3(14)
				C8	-C12	-C14	110.6(2)
				C13	-C12	-H121	108.2(14)
				C14	-C12	-H121	108.2(14)
				C12	-C13	-H131	109.5(15)
				C12	-C13	-H132	109.1(16)
				C12	-C13	-H133	111.5(16)
				H131	-C13	-H132	108(3)
				H131	-C13	-H133	109(2)

H132	-C13	-H133	110(2)
C12	-C14	-H141	106.3(17)
C12	-C14	-H142	113(2)
C12	-C14	-H143	108(2)
H141	-C14	-H142	106(3)
H141	-C14	-H143	107(3)
H142	-C14	-H143	117(3)

**Table S7** - Predicted  $^{13}\text{C}$  and  $^1\text{H}$  NMR shifts (ppm) in the iron complex **1** from a dimer calculation.

	$\delta_{\text{calc}}^{\text{dia}} (\mathbf{1})$	$\delta_{\text{calc}}^{\text{dia}} (\mathbf{1}) + \delta_{\text{calc}}^{\text{fc}} (\mathbf{1})$	$\delta^{\text{obs}} (\mathbf{2}) + \delta_{\text{calc}}^{\text{fc}} (\mathbf{1})$
C1	167	117	122.5
C2	-6	297	323.8
C3	144	139	132.8
C4	140	202	201.4
C5	115	13	22.5
C6	117	238	247.2
C7	116	-52	-44.3
C8	141	120	118.4
C9	13	-67	-51.4
C10	-1	87	113.4
C11	-5	64	92.3
C12	12	-42	-26.6
C13	-5	106	135.5
C14	0	28	52.9
H2	-4	3	9.6
H5	3	20	23.5
H6	5	-23	-21.5
H7	4	8	10.7
H9	-2	-2	2.7
H10	-3	-1	3.3
H11	-5	-7	-1.6
H12	-3	4	10.1
H13	-4	-2	3.5
H14	-3	-1	3.3

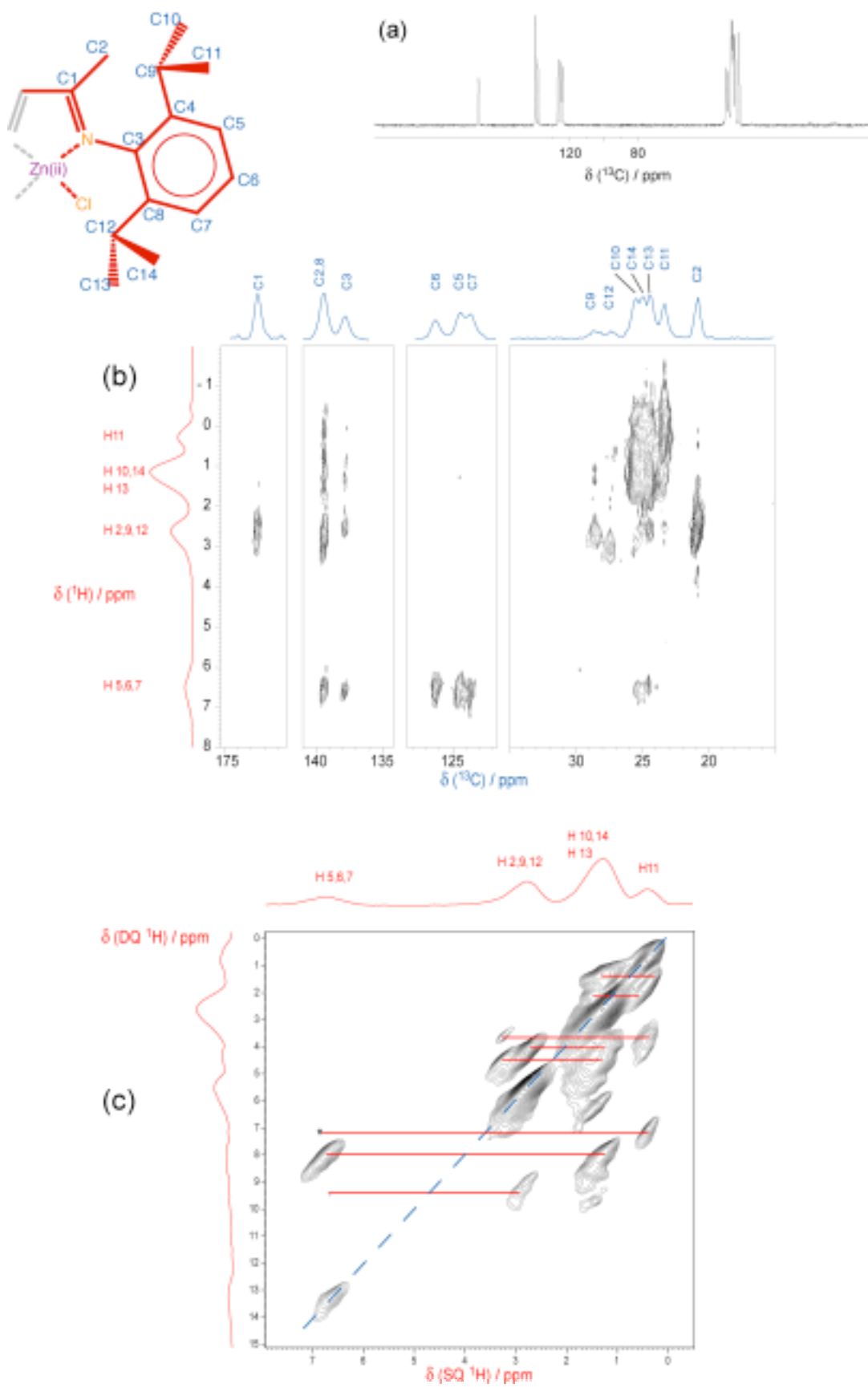


**Figure S1** - a)  $^{13}\text{C}$  MAS NMR spectra (500 MHz) of **2**; (b)  $^1\text{H}$ - $^{13}\text{C}$  dipolar HETCOR and (c)  $^1\text{H}$  DQ CRAMPS correlations of **2**.

All the spectra were acquired on compound **2** at a temperature of 30 deg under 20 kHz MAS. For a  $^1\text{H}$ - $^{13}\text{C}$  CP, a tangential amplitude modulated RF field<sup>(1)</sup> centered at 100 kHz was applied on  $^1\text{H}$ , while the carbon field on  $^{13}\text{C}$  was matched to obtain optimal signal; an optimal contact time was 1 ms. A decoupling field of 100 kHz was applied to protons according to the TPPM scheme<sup>(2)</sup> during acquisition. In a  $^1\text{H}$ - $^{13}\text{C}$  dipolar HETCOR experiment, 100 kHz windowless DUMBO-1<sub>22</sub> homonuclear dipolar decoupling<sup>(3)</sup> was applied during  $^1\text{H}$  evolution in  $t_1$ . A scaling factor of 0.58 during  $t_1$  was experimentally determined applying the same sequence on a standard  $^{13}\text{C}$ -uniformly labeled glycine sample. A total of 256  $t_1$  increments were collected ( $t_{1\max} = 32.7$  ms;  $t_{2\max} = 45$  ms), with 128 scans each and a recycle delay of 2.5 s (total recording time 23 h). Quadrature detection during  $f_1$  was achieved using the TPPI method.<sup>(4)</sup> An exponential line broadening of 10 Hz was applied in the two dimensions before Fourier transformation.

For a  $^1\text{H}$  DQ CRAMPS experiment,<sup>(5)</sup> double quantum excitation and reconversion were performed through two POST-C7<sup>(6)</sup> blocks of 42.8 us (corresponding to 3 basic POST-C7 elements each). Homonuclear  $^1\text{H}$  decoupling (100 kHz) was achieved by the DUMBO-1<sub>22</sub> scheme<sup>(3)</sup> during  $f_1$  as described for experiment (a), while a windowed w-DUMBO-1 homonuclear decoupling scheme<sup>(7)</sup> was applied during  $t_2$  acquisition. The scaling factors for DUMBO-1 during  $f_1$  and  $f_2$  were determined experimentally as 0.58 and 0.84, respectively. A total of 80  $t_1$  increments were collected ( $t_{1\max} = 8.4$  ms;  $t_{2\max} = 13.7$  ms), with 48 scans each and a recycle delay of 2 s (total recording time 2 h). Quadrature detection during  $f_1$  was achieved using the States-TPPI method. An exponential line broadening of 10 Hz was applied in the two dimensions before Fourier transformation.

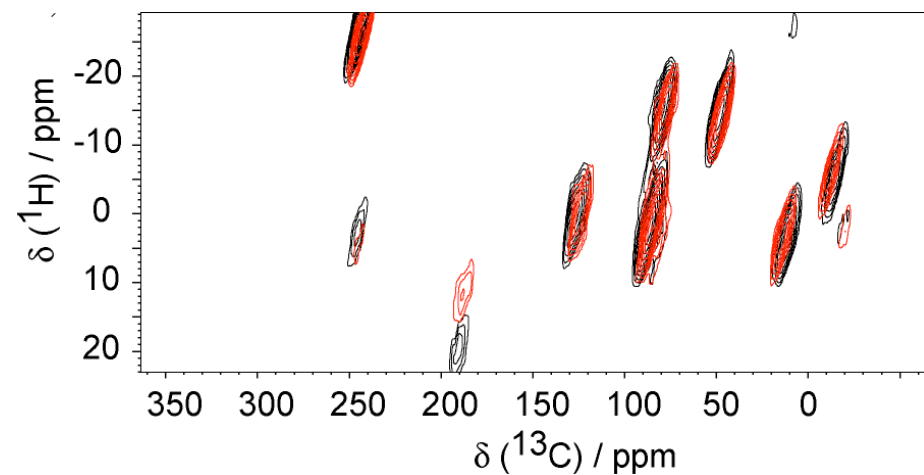


**Figure S2** - Comparison between two rotor-synchronized  $^1\text{H}$ - $^{13}\text{C}$  TEDOR correlations of **1**, acquired under 33 kHz (black contours) and 30 kHz (red contours) MAS ( $T=303$  K;  $B_0=11.7$  T). The comparison allows the correct evaluation of the shift of the C2-H2 group, which is aliased, and moves 3 kHz upfield upon changing the MAS rate.

The assignment of the  $\text{C}_2\text{H}_2$  signal was also confirmed by recording the same experiment on a sample selectively  $^2\text{H}$ -labeled on the  $\alpha$ -imine methyl (kindly provided by P.J Chirik).

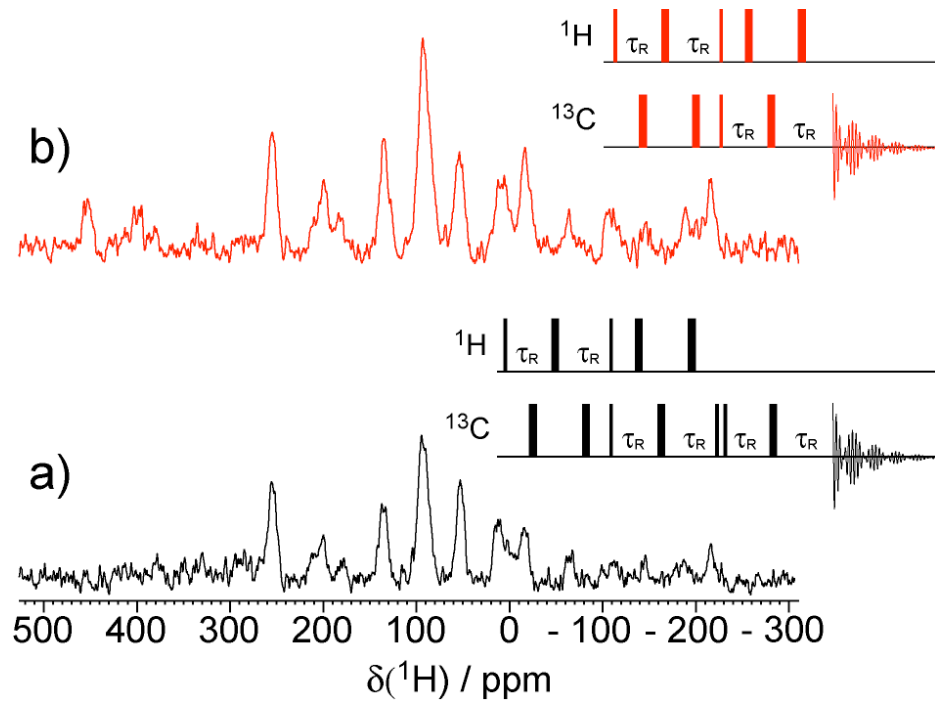


**Figure S3** - Comparison between a standard <sup>1</sup>H-<sup>13</sup>C TEDOR correlation of **1** (a) and a modified version, lacking the z-filter and spin-echo elements before <sup>13</sup>C acquisition (b). ). Narrow and wide rectangles denote 90° and 180° pulses, respectively;  $\tau_R$  represents the rotor period. (33 kHz MAS; T=303 K; B<sub>0</sub>=11.7 T).

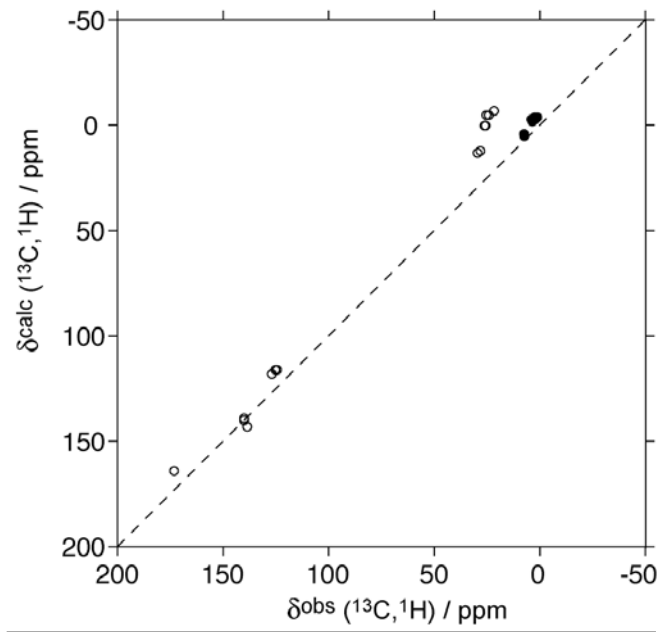


**Figure S4** - Correlation between experimental shifts for complex **2** and calculated diamagnetic shifts for complex **1**. <sup>13</sup>C are represented by open symbols and <sup>1</sup>H by filled symbols.

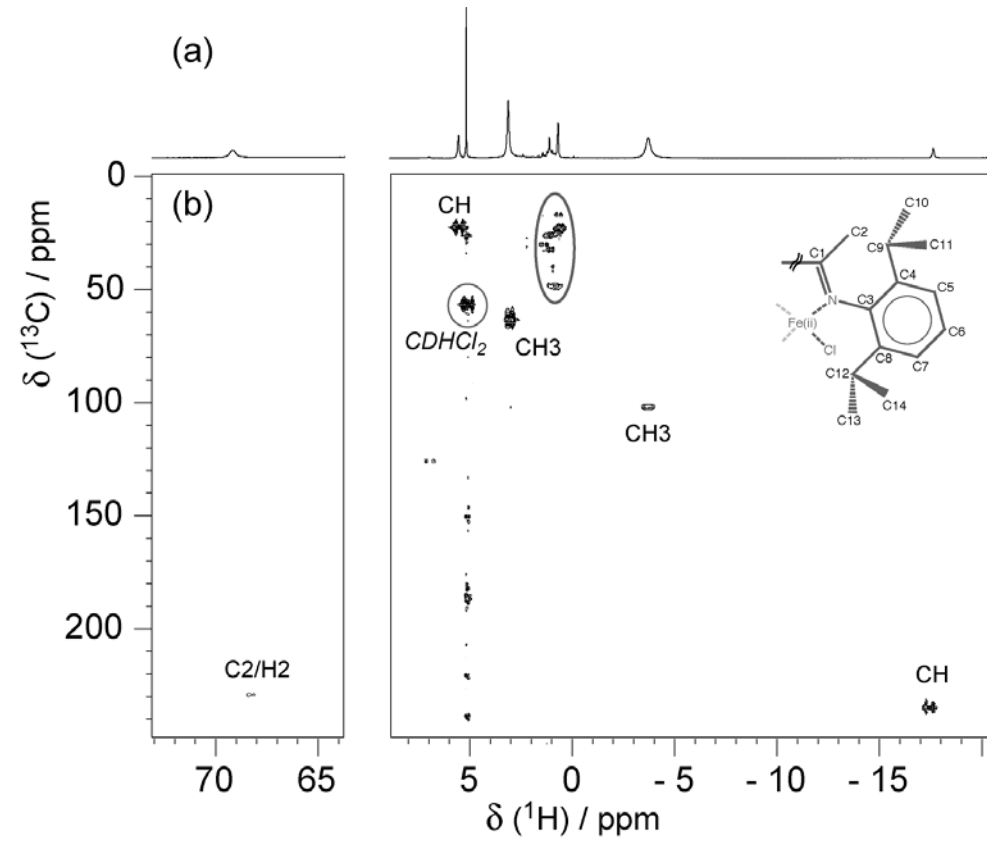


**Figure S5** - Liquid-state NMR spectra of **1** dissolved in  $\text{CH}_2\text{Cl}_2$ . (a)  $^1\text{H}$  NMR; (b)  $^1\text{H}, ^{13}\text{C}$ -HMQC. The spectra were recorded at 30 deg on a Varian Inova 500 NMR spectrometer using the following parameters:  $t_{1\max} = 50$  ms;  $t_{2\max} = 150$  ms, 120 ppm sweep width in the  $^1\text{H}$  dimension, total recording time 64 h. Quadrature detection during  $f_1$  was achieved using the States method. Transverse relaxation during the pulse sequence due to paramagnetism was minimized by reducing the MQC excitation delay to 1.1 ms. Resonances are labeled according to the  $^1\text{H}$  assignment reported by Bart et al. (8). Two circles identify the residual solvent signals, as well as cross-peaks from the uncomplexed, diamagnetic ligand.

## Bibliography

- (1) Hediger, S.; Meier, B. H.; Kurur, N. D.; Bodenhausen, G. and Ernst, R. R., Nmr Cross-Polarization by Adiabatic Passage through the Hartmann-Hahn Condition (Aphh). *Chem. Phys. Lett.* **1994**, *223*, 283-288.
- (2) Bennett, A. E.; Rienstra, C. M.; Auger, M.; Lakshmi, K. V. and Griffin, R. G., Heteronuclear Decoupling in Rotating Solids. *J. Chem. Phys.* **1995**, *103*, 6951-6958.
- (3) De Paepe, G.; Elena, B. and Emsley, L., Characterization of heteronuclear decoupling through proton spin dynamics in solid-state nuclear magnetic resonance spectroscopy. *J. Chem. Phys.* **2004**, *121*, 3165-80.
- (4) Marion, D. and Wüthrich, K., Application of phase sensitive two-dimensional correlated spectroscopy (COSY) for measurements of  $^1\text{H}$ - $^1\text{H}$  spin-spin coupling constants in proteins. *Biochem Biophys Res Commun* **1983**, *113*, 967-74.
- (5) Brown, S. P.; Lesage, A.; Elena, B. and Emsley, L., Probing proton-proton proximities in the solid state: high-resolution two-dimensional  $^1\text{H}$ - $^1\text{H}$  double-quantum CRAMPS NMR spectroscopy. *J. Am. Chem. Soc.* **2004**, *126*, 13230-1.

- (6) Hohwy, M.; Jakobsen, H. J.; Eden, M.; Levitt, M. H. and Nielsen, N. C., Broadband dipolar recoupling in the nuclear magnetic resonance of rotating solids: A compensated C7 pulse sequence. *J. Chem. Phys.* **1998**, *108*, 2686-2694.
- (7) Lesage, A.; Sakellariou, D.; Hediger, S.; Elena, B.; Charmont, P.; Steuernagel, S. and Emsley, L., Experimental aspects of proton NMR spectroscopy in solids using phase-modulated homonuclear dipolar decoupling. *J Magn Reson* **2003**, *163*, 105-13.
- (8) Bart, S. C.; Hawrelak, E. J.; Schmisser, A. K.; Lobkovsky, E.; Chirik, P. J., Synthesis, reactivity and solid-state structures of four-coordinate iron(II) and manganese(II) alkyl complexes. *Organometallics* **2004**, *23*, 237.

**Complete ref. 44 from the Main Text**

- (44) Gaussian 03, Revision C.02; Frisch, M. J.; Trucks, G. W.; Schlegel, H. B.; Scuseria, G. E.; Robb, M. A.; Cheeseman, J. R.; Montgomery, J., J. A.; Vreven, T.; Kudin, K. N.; Burant, J. C.; Millam, J. M.; Iyengar, S. S.; Tomasi, J.; Barone, V.; Mennucci, B.; Cossi, M.; Scalmani, G.; Rega, N.; Petersson, G. A.; Nakatsuji, H.; Hada, M.; Ehara, M.; Toyota, K.; Fukuda, R.; Hasegawa, J.; Ishida, M.; Nakajima, T.; Honda, Y.; Kitao, O.; Nakai, H.; Klene, M.; Li, X.; Knox, J. E.; Hratchian, H. P.; Cross, J. B.; Adamo, C.; Jaramillo, J.; Gomperts, R.; Stratmann, R. E.; Yazyev, O.; Austin, A. J.; Cammi, R.; Pomelli, C.; Ochterski, J. W.; Ayala, P. Y.; Morokuma, K.; Voth, G. A.; Salvador, P.; Dannenberg, J. J.; Zakrzewski, V. G.; Dapprich, S.; Daniels, A. D.; Strain, M. C.; Farkas, O.; Malick, D. K.; Rabuck, A. D.; Raghavachari, K.; Foresman, J. B.; Ortiz, J. V.; Cui, Q.; Baboul, A. G.; Clifford, S.; Cioslowski, J.; Stefanov, B. B.; Liu, G.; Liashenko, A.; Piskorz, P.; Komaromi, I.; Martin, R. L.; Fox, D. J.; Keith, T.; Al-Laham, M. A.; Peng, C. Y.; Nanayakkara, A.; Challacombe, M.; Gill, P. M. W.; Johnson, B.; Chen, W.; Wong, M. W.; Gonzalez, C. and Pople, J. A.; Gaussian, Inc., Wallingford CT, 2004.